Federated EGSV-AACO for Decentralized Spectrum Sensing and Sharing in IoT Networks

Jing Ling
School of Integrated Circuits and Communications, SuZhou Institute of Industrial Technology, Suzhou, Jiangsu, 215104, China
E-mail: lingjing68@hotmail.com

Keywords: extreme gradient support vector with adaptive ant colony optimization (EGSV-AACO), Internet of Things (IoT), privacy problems, smart campus network, spectrum sharing

Received: September 9, 2025

Wireless bandwidth is in greater demand than ever before due to the Internet of Things' (IoT) applications' rapid expansion in fields including smart cities, autonomous and Industry 4.0. Traditional fixed spectrum allocation approaches can lead to inefficient utilization and excessive interference levels, particularly in densely populated areas. The purpose of this evaluation is to create an intelligent, decentralized, and privacy-preserving framework for optimizing spectrum detection and sharing among IoT devices utilizing machine learning (ML) techniques. The Cognitive Radio Networks (CRNs) Dataset is gathered from the Kaggle source. The procedure consists of four sequential steps. Each IoT node uses Extreme Gradient Support Vector with Adaptive Ant Colony Optimization (EGSV-AACO) to monitor spectrum occupancy and identify idle bands. Each node builds a local spectrum access model based on temporal spectrum patterns. Model weights are delivered to a nearby edge server on a regular basis to avoid exposing raw data using Federated Averaging (FedAvg). The server aggregates the locally trained models to form a global model and redistributes it to all participating devices. This updated global model will drive real-time, collision-free spectrum allocation among IoT devices. A smart campus simulation using MATLAB shows that the proposed EGSV-AACO framework ensures access convergence, improves spectrum usage, and prevents raw data leakage. The developed model outperforms all baseline methods and achieved an accuracy of 97%, precision of 97.5%, recall of 96%, and an F1-score of 96.5%. Overall, this research introduces a novel Federated EGSV-AACO framework that significantly enhances decentralized, privacy-preserving, and intelligent spectrum sensing and sharing in IoT networks.

Povzetek: Raziskava predstavlja federativni okvir EGSV-AACO, ki z decentraliziranim strojnim učenjem omogoča natančno, zasebnostno ohranjajoče in učinkovito zaznavanje ter deljenje radijskega spektra v IoT omrežjih.

1 Introduction

Internet of Things (IoT) explosive growth has revolutionized contemporary society by establishing a networked ecosystem in which billions of individual items can easily communicate with other objects [1]. IoT applications, such as smart cities, intelligent transportation systems, industrial automation, and are constantly altering the methods for collecting, communicating, and using data [2]. Effective and reliable communication frameworks that can support a variety of services in real time are necessary due to the increasing interconnectedness [3]. The role of wireless spectrum in this research is critical as it is the essential material of communication among IoT devices [4].

As the number of IoT devices has increased exponentially and rapidly, spectrum resources have become as much in demand as never before. In comparison to the traditional communication networks that rely on pre-determined frequency allocation, IoT ecosystems are very dynamic and comprise of a wide range of devices that have different communication needs [5,6]. The existing wireless infrastructure is currently experiencing a massive amount of pressure, particularly in densely populated regions such as campuses, cities and industrial hubs due to its dynamic nature. Spectrum management is essential in enabling scalability and sustainability of IoT-driven services besides provision of continuous connection [7, 8].

Spectrum utilization, in this case, denotes a fair and dynamic usage of the existing resources and the alternation of frequency bands [9]. While overloaded frequencies result in interference, delays, and a lower quality of service, idle or underused spectrum indicates missed communication possibilities [10]. Thus, making the most use of the spectrum that is available is essential to the development of IoT. Furthermore, since devices continually create and process data across several domains, the scattered and data-intensive nature of IoT networks adds another level of complexity [11]. The real difficulty is how to manage the few spectrum resources for the growth of IoT devices. Fixed allocations tend to be inefficient and disruptive, particularly in an environment with high assignments density. To achieve this kind of fair real-time access, and at the same time, security and privacy, innovative approaches need to be used that are scalable, adaptable, and reliable without affecting the performance of communication and the protection of data.

Therefore, the present research focuses on creating a decentralized and intelligent spectrum management system designed for real-time, secure, and effective resource allocation in order to overcome these constraints and satisfy the growing communication demands of IoT contexts.

This research investigates three key research questions (RQ):

RQ1: *Can EGSV-AACO accurately detect idle spectrum bands under dynamic IoT traffic conditions?*

RQ2: *Does FedAvg improve detection reliability compared to centralized training?*

RQ3: *Can the proposed hybrid model improve accuracy and reduce interference compared to other existing approaches?*

The proposed Extreme Gradient Support Vector with Adaptive Ant Colony Optimization (EGSV-AACO) model accurately detected idle spectrum bands in dynamic IoT environments and evaluated whether Federated Averaging (FedAvg)-based decentralized learning improved reliability over centralized methods. The hybrid model also assessed overall performance gains compared to other existing approaches. In general, the research provides a smart, decentralized, privacy-preserving system for efficient IoT spectrum sharing. The significant contribution of the research is as follows:

i. **Dataset Integration:** A comprehensive CRN spectrum-sensing dataset is used, incorporating interference levels and temporal usage patterns.
ii. **Data Preprocessing:** Min–Max normalization ensures stable training and reduces feature-scale imbalance.
iii. **Privacy-Preserving Learning:** FedAvg enables decentralized learning without sharing raw data, enhancing privacy and security.
iv. **Advanced Spectrum Sensing:** EGSV-AACO improves detection accuracy, reliability, and dynamic spectrum allocation, outperforming traditional methods.

2 Literature review

Recent research on dynamic spectrum access and sharing has primarily been aimed at increasing the effectiveness, security, and privacy of wireless networks and the IoT. However, prior methods suffered from scalability, complexity, and resilience limitations, despite investigations into strategies such as blockchain, federated learning, and reinforcement learning (Table 1).

Table 1: Evaluation of related works on spectrum access approaches

Citation	Objective	Method	Outcome	Limitations
Wang et al. [12]	Reduce Vehicular Ad Hoc Nestwork (VANET) channel conflict using optimized spectrum access	Deep Reinforcement Learning (DRL) + Depth-First Search (DFS)	Fewer collisions probability 60% and reduce packet loss 0.8 to 0.1	Limited scalability in dense vehicular networks
Grissa et al. [13]	Ensure anonymous and secure Citizens Broadband Radio Service (CBRS) spectrum access privacy	Blockchain + Crypto	Strong privacy with secure operations	High computation and increased system complexity
Chang et al. [14]	Improve Dynamic Spectrum Access (DSA) using collaborative multi-agent learning framework	Federated Multi-Agent Deep Reinforcement Learning (Fed-MADRL)	Reduced overhead and preserved privacy	Slow convergence under complex environments
Kaur et al. [15]	Enhance DSA reliability under noisy feedback channels	Gated Recurrent Unit (GRU)- Deep Reinforcement Learning (DRL)	Improved resilience and accuracy 91% results	Difficult cooperative decisions with noisy feedback
Zhang et al. [16]	Achieve distributed DSA using local-only observations effectively	Multi-agent Deep Q-Network (DQN)	High performance 90% over random baselines	Needs offline global training information
Amrallah et al. [17]	Optimize Unmanned Aerial Vehicle (UAV) monitoring with efficient power selection	Multi-Armed Bandit (MAB) algorithms	Better data-rate 30 UAV and	No UAV cooperation

			interference handling	limits decisions
Makhdomi et al. [18]	Enable secure Wireless Service Provider (WSP) spectrum sharing with incentives	Blockchain (DSA)	Improved security and sensing performance	Higher latency and computational overhead
Chen et al. [19]	Maximize Vehicle-to-Infrastructure (V2I)/ Vehicle-to-Vehicle (V2V) capacity in Reconfigurable Intelligent Surface (RIS)-aided networks	Block Coordinate Descent (BCD)-based	Enhanced Quality of Service (QoS) in dynamic channels probability in 0.9	Depends on near-optimal estimated solutions
Gu et al. [20]	Improve Low Earth Orbit (LEO) satellite spectrum sharing efficiency	LEO collaboration	Higher efficiency 89% and convergence 87% achieved	Increased coordination complexity in networks

The experiment [21] is designed to investigate the possibilities and challenges of the future of the IoT with the integration of 5G/6G, zero-trust security, and blockchain to achieve the universal connection and secure access. The approach suggested a blockchain-based authentication system (BasIoT) and a zero-trust security architecture for IoT devices. Although the framework identifies fascinating research opportunities to safe, ubiquitous IoT, it has weaknesses in scalability and complexity of implementation.

Enhancing safe spectrum sharing and power allocation in V2V communications against eavesdropping was the objective of the research [22]. Using cooperative decision-making and multi-agent reinforcement learning, the technique optimizes power, frequency, and the deployment of friendly jammers. Increased system complexity and dependence on cooperating agents were drawbacks; however, simulations have shown that the approach was more secure and resilient than current approaches.

Enhancing safe spectrum sharing in intelligent IoT networks against jamming and emulation assaults is the objective of the research [23]. The approach examined current defenses and suggested online machine learning (ML)-based attack and defensive tactics, such as channel access restrictions that take sensing delays into account and time-varying feedback graph models. Vulnerability to adaptable attackers was a drawback.

Improved Convolutional Neural Networks (CNNs) and Kernel Principal Component Analysis (KPCA) were being used in the research [24] to improve spectrum detection in Internet of Vehicle (IoV) communication. KPCA extracted features by mapping signals to a high-dimensional space, whereas CNN classifies with less complexity. The results indicated a 10% increase in accuracy compared to LeNet5, Elman, and SVM. Limitation: The approach function is largely determined by the quality and conditions of the offline training phase.

Evaluation of user performance in huge cognitive radio networks (CRNs) was used a hybrid spectrum access model that combines overlay and underlay schemes was the goal of the examination [25]. Simulations were used to support the analysis of the age of information (AoI), throughput, and success probability using stochastic geometry. The results demonstrate that hybrid access performs noticeably better than separate approaches. Modeling assumptions has the potential to oversimplify real-world processes, which was a restriction.

2.1 Research gaps

Prior studies, including works such as [12], [14], [17], and [23], exhibit key limitations, including high computational cost, restricted scalability in dense IoT networks, dependence on centralized learning, and privacy risks due to raw data exchange. Methods also struggle with noisy feedback [15], slow convergence [14], blockchain overhead [13], and limited cooperative decision-making efficiency. Optimization techniques remain incomplete, and adaptability to dynamic spectrum patterns is insufficient. The developed EGSV-AACO with FedAvg addresses these gaps by using decentralized learning, aggregation protection privacy, robust hybrid optimization, and much better sensing accuracy and reliability.

2.2 Problem statement

Past research has considered privacy-preserving approaches to spectrum sharing, significant obstacles still need to be addressed. For example, the primary disadvantage of the research was the fact that whereas TSAS [13] raised privacy and security, it could have had the problem of computation load, latency, and scaling applications in larger settings. A key limitation was that despite the increased accuracy of KPCA-CNN [24], such an approach cannot be adapted well to the highly dynamic nature of the IoV environment, as it involves offline training. Online retraining has a high computation overhead, and the model might not learn well when

exposed to previously unseen noise patterns, spectrum heterogeneity, or a large-scale deployment that needs faster online adaptation.

The suggested EGSV-AACO with the FedAvg framework mitigates the shortcomings of the existing research. It features lightweight, secure, and scalable IoT devices with the ability to endure such a large ecosystem, ensuring that computation is reduced and that the model can be aggregated, thus preventing the trickle of raw data in the presence of decentralized federated learning and adaptive spectrum sensing.

3 Methodology

The implementation of the methodology combines a hybrid intelligence model of spectrum sensing and decentralized optimization. First, a dataset of Cognitive Radio Network (CRN) spectrum sensing data was obtained with signal, environmental, and network characteristics. Stable training involved Min-Max normalization of the values. Each IoT device used an EGSV-AACO to identify idle spectrum bands and to adjust parameters adaptively. Local models were then consolidated via FedAvg, but the privacy was guaranteed by sharing ordinary weights, rather than raw data. This method has made it possible to have precise, safe, and scalable spectrum distribution within IoT networks. Figure 1 illustrates the workflow of the proposed research.

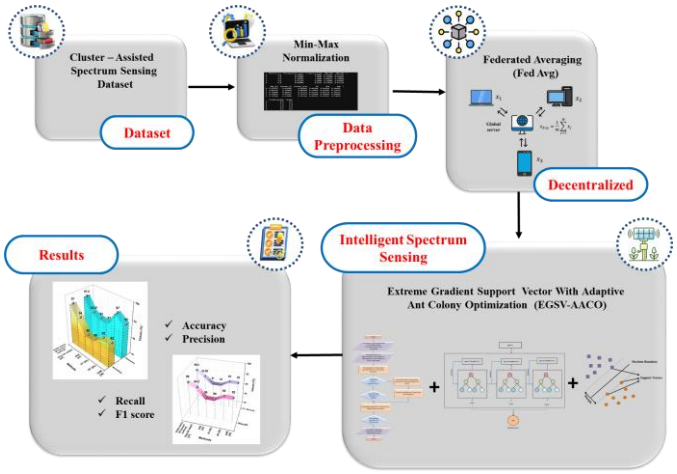

Figure 1: EGSV-AACO for intelligent spectrum sensing in IoT environments

3.1 Dataset

The dataset Cognitive Radio Networks (CRNs) is gathered from the publiclay available Kaggle source (https://www.kaggle.com/datasets/ziya07/cluster-assisted-spectrum-sensing-dataset), this CRNs dataset is optimized towards research in the area of Cluster-Assisted Spectrum Sensing Dataset, specifically on cluster-assisted spectrum sensing. It contains 1000 data samples, It offers a holistic ensemble of features that characterizes properties of signals, dynamic actions of the environmental context, and the network operations to enable effective spectrum sensing and decision-making. The dataset supports ML–based tasks such as primary user detection, spectrum availability prediction, and interference minimization. For 30% testing ratio and 70% of training the dataset was spitted. Table 2 summarizes the central categories of features and target variable available in the CRNs spectrum sensing dataset.

Table 2: Core attributes of the CRN's spectrum sensing dataset

Category	Attributes
Signal Characteristics	Power Spectral Density (PSD), Signal-to-Noise Ratio (SNR), and Received Signal Strength Indicator (RSSI)
Environmental Conditions	Noise level, Interference levels, Channel quality
Network Metrics	Cluster ID, Sensing duration, Transmission success rate
Temporal Features	Time of spectrum sensing, Periodicity of spectrum availability
Target Variable	Binary: 0 = Spectrum Unavailable, 1 = Spectrum Available; or Multiclass based on interference levels

3.2 Min-max normalization

This normalization is used to ensure consistent scaling for features such as RSSI, SNR, and PSD. This is performed by assigning each value to a defined range, normally $[0,1]$, while preserving the relationships between the elements. The normalized value x' is described as follows in equation (1).

$$x' = \frac{x - \min_B}{\mathrm{Max}_B - \mathrm{Min}_B} (\mathrm{new\_Max}_B - \mathrm{new\_Min}_B) \quad (1)$$

Where $\mathrm{new\_Max}_B$ and $\mathrm{new\_Min}_B$ provide the desired range, Max_B and Min_B are the feature's maximum and minimum values, and x is the original feature value. This enhances the forecast of spectrum availability and stabilizes model training.

3.3 Federated averaging (fedavg)

In the proposed framework, the spectrum sensing date uploaded by each IoT device (local client) would be used

to train the model and the weights would be updated and sent to the global server. These updates are securely aggregated by the server in a FedAvg way by obtaining the global model (x_{Avg}) as a weighted average in equation (2).

$$x_{Avg} = \frac{1}{m}\sum_{j=1}^{M} x_j \quad (2)$$

M defines total number of IoT devices (local clients), x_j local model parameters (weights), and m defines the number of data samples. This enhances spectrum allocation and detection across IoT networks while guaranteeing privacy-preserving, decentralized optimization. Figure 2 illustrates the FedAvg framework.

Figure 2: FedAvg Framework for IoT devices

The technique in the suggested framework is to actively optimize spectrum allocation across several IoT devices without disclosing their private raw data. Every IoT node l maintains track of a local dataset. D_l is the local dataset stored on IoT device l.

$$D_l \triangleq \left\{\left(w_{l,n}, z_{l,n}\right)\right\}_{n=1}^{m_l} \quad (3)$$

m_l is the number of training samples available on the device. Where equation (3) $z_{l,n}$ stands for spectrum allocation choices and $w_{l,n}$ for device characteristics (such as channel condition and traffic demand). n is the sample index. The goal of global optimization is equation (4).

$$\min_x\{E(x) \triangleq \sum_{l=1}^{M} o_l E_l(x)\} \quad (4)$$

The spectrum allocation error is represented by the local loss function at device l, $E_l(x)$. $\min_x$ is the optimization objective: find the model parameters x (allocation variables vector) that minimize the global loss function. The global loss function for every device was denoted by $\sum_{l=1}^{M} o_l$. E(x) is the global loss function, which measures the total spectrum allocation error across all IoT devices. The Allocation variables vector (model parameters for spectrum optimization) is represented by $x \in \mathbb{R}^N$. The Loss function for the sample $(w_{l,n}, z_{l,n})$ is defined by $\ell(x; w_{l,n}, z_{l,n})$. The traditional distributive stochastic gradient descent (SGD) technique serves as the foundation for FedAvg. SGD was used to modify local models, as determined in equation (5).

$$x_{s+1}^l \leftarrow x_s^l - \eta_s \Delta E_l(x_s^l; \xi_s^l, a) \quad (5)$$

The iteration number (communication round) was denoted by s. x_{s+1}^l denotes the updated local model parameters of device l after the $s+1$ -th training iteration (communication round). At iteration s, x_s^l defines the device l local model parameters. The learning rate (step size) at iteration s was denoted by η_s. The Mini-batch size for local updates was a . $\Delta E_l(x_s^l; \xi_s^l, a)$ was the Mini-batch gradient of device l, and ξ_s^l was the Mini-batch generated from the local dataset D_l at iteration s. And combined on the server by the following equation (6).

$$\bar{x}_{s+1} = \sum_{l=1}^{M} o_l x_{s+1}^l \quad (6)$$

Following the server-side averaging of local models, $\bar{x}_{s+1}$ was the aggregated global model. FedAvg is employed to aggregate on a global level with other local updates of IoT models without exchanging raw spectrum sensing data.

3.4 Extreme gradient support vector with adaptive ant colony optimization (EGSV-AACO)

The proposed research will utilize the EGSV-AACO algorithm as the core intelligence-based spectrum sensing mechanism at the IoT node level. EGSV is trained to categorize the spectrum bands as idle or occupied by learning the temporal signature of each band, whereas AACO adapts the model parameters to maximize accuracy in the uneven environment. This hybrid integration enables each IoT device to efficiently locate spectrum resources, adjust to time-varying spectrum, and reduce false alarms that can cause collisions. The resulting locally optimized spectrum access models produced by EGSV-AACO are then aggregated via Federated Averaging (FedAvg) to assemble a global model, which is decentralized, privacy-preserving, and efficient for spectrum sharing across IoT networks. Algorithm 1 describes the process of the EGSV-AACO method.

Algorithm 1: $EGSV - AACO\ Procedure$

$\%\ Goal: Hybrid\ XGBoost\ +\ SVM\ +\ Adaptive\ ACO\ +\ Federated\ Aggregation$

1. $Initialize\ IoT\ nodes\ (N)\ and\ spectrum\ bands\ (S)$
2. $Initialize\ pheromone\ matrix\ Tau(S,S), AACO\ params\ (alpha, beta, rho, R)$
3. $Initialize\ EGSV\ params\ (numTrees, learningRate, kernelType)$
4. $For\ each\ node\ and\ band\ \rightarrow\ extract\ feature\ vector\ w\_j\ and\ label\ z\_i$
5. $Train\ XGBoost\ using\ (w\_j\ , z\_i)\ to\ generate\ boosted\ features$
6. $Train\ SVM\ using\ boosted\ features\ to\ obtain\ EGSV\ classifier$
7. $For\ each\ band\ \rightarrow\ predict\ local\ state\ using\ EGSV\ \rightarrow\ store\ localPrediction$
8. $Initialize\ bestCost\ =\ \infty\ and\ bestHyperParams\ =\ default$
9. $For\ iter\ =\ 1:\ maxIterations\quad \%\ AACO\ tuning\ loop$
10. $\quad For\ each\ ant\ =\ 1:\ numAnts$
11. $\quad\quad Construct\ spectrum\ path\ using\ transition\ probability\ rule:$

$\quad\quad p(i)\ =\ (Tau(i)\text{^}alpha\ *\ Heuristic(i)\text{^}beta)\ /\ \Sigma(all\ feasible)$

12. $\quad\quad Compute\ path\ cost\ =\ Collision\ +\ Interference\ +\ Classification\ Error$
13. $\quad\quad Update\ DeltaTau\ based\ on\ (R\ /\ pathCost)$
14. $\quad\quad If\ pathCost\ <\ bestCost\ \rightarrow\ update\ bestHyperParams\ =\ current\ set$
15. $\quad End$
16. $\quad Evaporate\ pheromone: Tau\ =\ rho\ *\ Tau\ +\ DeltaTau$
17. $\quad Optionally\ adjust\ (alpha, beta)\ for\ dynamic\ environment$

$\quad End$

18. $Update\ EGSV\ model\ hyperparameters\ using\ bestHyperParams$
19. $Collect\ all\ trained\ local\ models\ \rightarrow\ apply\ FedAvg\ \rightarrow\ get\ globalModel$
20. $For\ each\ node\ and\ spectrum\ band:$
21. $\quad finalState(band)\ =\ globalModel.predict(extract\_features(node, band))$
22. $Output\ finalState\ as\ optimized\ spectrum\ allocation\ map$

3.4.1 Extreme gradient support vector (EGSV)

The hybrid learning algorithm used incorporates a combination of Extreme Gradient Boost (XGBoost) and SVM, known as the EGSV, to enhance the spectrum sensing accuracy. The XGBoost was used to acquire higher-level spectral features applied in addition to classify the decision boundary more robustly, whereas SVM is employed in a more robust classification of occupied and idle frequency bands. By integrating the gradient boosting feature of XGBoost and the powerful generalization ability of SVM, EGSV can address dynamically changing spectrum environments adequately, and IoT devices can run more predictable and adaptable local spectrum detection.

XGBoost

XGBoost is a robust and scalable technique that has been successfully applied to a wide range of tasks involving regression and classification. It is used in this research as an extension to the EGSV approach to carry out the process of spectrum sensing and occupancy prediction over IoT-enabled networks. The objective is to categorize spectrum bands as idle (available) or occupied (busy) and then optimally allocate resources, whether it is spectrum or wireless resources.

The XGBoost model is an ensemble model that is made up of numerous classification and Regression Trees (CART) regressors. Figure 3 (a) shows the tree structure of XGBoost consisting of a root nodes, internal nodes, leaf nodes, and branches. In spectrum sensing, all IoT devices contribute feature data, which includes the levels of signals, variance in noise, and temporal uses. The CARTs transmit these features, and internal nodes make binary decisions, branch points drive predictions of the state of the spectrum, and leaves predict the final result

of classification. The ensemble prediction of all trees gives the detection outputs of the XGBoost model.

The model is represented by the following equation (7) on the j^{th} data instance (w_j, z_i), such that w_j is the extracted signal features and z_i refers to the actual occupancy label (idle/busy).

$$\hat{z}_i = \alpha \sum_{l=1}^{L} e_l(w_j) \quad (7)$$

Where $\hat{z}_i$ is the estimated spectrum state caused by i, where w_j is the prior input information of the model, the learning rate is α, L is the values of CART used, and $e_l(w_j)$ is the result of the l^{th} regression tree. Equation (7) shows that the overall classification is performed by collecting all regression tree outputs. The objective function K is defined by the following equation (8).

$$K = \sum_{j=1}^{m} k(z_j, \hat{z}_j) + \sum_{l=1}^{L} \Omega(e_l) \quad (8)$$

In this circumstance l, which is the loss function, computes the prediction error between the actual occupancy state z_j and the predicted state $\hat{z}_j$. Objective function (K), Sample index (j), Total samples (m), Loss functions $k(z_j, \hat{z}_j)$, Number of trees (L), and Tree regularization $\Omega(e_l)$.

The regularization penalty Ω(e) penalizes very complicated tree shapes, thereby boosting the generalization capacity of spectrum forecasting models in changeable IoT contexts. In each CART, the regularization equation (9) is formulated as follows:

$$\Omega(e) = \gamma^S + \frac{1}{2}\lambda \sum_{i=1}^{S} \omega_i^2 \quad (9)$$

In this equation, (S) represents the total number of leaf nodes, (ω_i) is the projected value at the (i^{th}) leaf node, $(\gamma^S)$is the complexity penalty based on leaf count. (γ) and (λ) are regularization coefficients to prevent overfitting in quickly changing spectrum data. The XGBoost model is trained in a step-by-step fashion to maximize spectrum classification performance. New CARTS are created in every iteration and combined with previously created CARTS to reduce the error of detection. The second-order Taylor series expansion is used to redefine the objective function, as shown in equations (10-12). These equations incorporate the first- and second-order gradients: Equation (11) indicates the direction of the error, while equation (12) provides confidence in the update,

$$K^{(s)} = \sum_j [k(z_j, \hat{z}_j^{(s-1)}) + h_j e_s(w_j) + \frac{1}{2} g_j e_s^2(w_j)] + \Omega(e_s) + d \quad (10)$$

$$h_j = \frac{\partial k\left(z_j, \hat{z}_j^{(s-1)}\right)}{\partial \hat{z}_j^{(s-1)}} \quad (11)$$

h_j is the first-order gradient, which measures how sensitive the loss function is to small changes in the prediction. g_j is the second-order gradient. $K^{(s)}$ computes the objective function at iteration s. $\Omega(e_s)$is the regularization penalty for the new tree, and $d$is a constant. $e_s(w_j)$ is the Prediction of $s-th$ tree. $e_s^2(w_j)$ is the Squared tree output, j is the sample index, w_j is the output weight $k(z_j, \hat{z}_j^{(s-1)})$ is the loss function, comparing the true label z_j (actual spectrum state: idle/busy) and the predicted value $\hat{z}_j^{(s-1)}$ from the previous iteration. z_j is the true spectrum occupancy label of the jth sample. $\hat{z}_j^{(s-1)}$ is the predicted spectrum occupancy of the jth sample in the $(s-1)$-th iteration. ∂ derivative operator, meaning we're calculating the slope of the loss curve at that point.

$$g_j = \frac{\partial^2 k\left(z_j, \hat{z}_j^{(s-1)}\right)}{\left(\partial \hat{z}_j^{(s-1)}\right)^2} \quad (12)$$

g_j is also called curvature information, which measures how steep or flat the loss curve is around the prediction. ∂ is the derivative operator, Again, $k\left(z_j, \hat{z}_j^{(s-1)}\right)$ is the loss function between actual state z_j and predicted state $\hat{z}_j^{(s-1)}$. ∂^2 is the second derivative, meaning we're looking at the curvature (bending) of the loss function.

These gradients direct the optimization by updating the weak learners to reduce misclassification of idle and occupied channels. $K^{(s)}$ is the objective function at iteration s. h_j defines the loss's first-order gradient (error sensitivity). g_j is the second-order gradient (curvature information), and $e_s(w_j)$ is the prediction of the updated tree at iteration s.

It is in this research that a residual standard error (RSE) is employed as the measure of loss in evaluating predictability. Each example w_j (signal feature vector) is assigned to a leaf node, and the regression function can be expressed in equation (13).

$$e_l(w_j) = \omega_{q(w_j)}, \omega \in \mathbb{R}^S, r(w_j): \mathbb{R}^c \to \{1,2,\dots,S\} \quad (13)$$

$e_l(w_j)$is the output of the l^{th} regression tree for input w_j, whereas $\omega_{q(w_j)}$ is the leaf weight (prediction score) for input w_j. $r(w_j)$ is the leaf assignment function, which maps input w_j to a leaf node index. $\mathbb{R}^S$ is the S real-number components. $\mathbb{R}^c$ refers to the number of input characteristics. S was the number of leaves on the tree. Finally, using $H_i = \sum_{j \in I_i} h_j$ and $G_i = \sum_{j \in I_i} g_j$, the optimum solution of the objective function, it could be defined as equation (14).

$$K_{min} = -\frac{1}{2} \sum_{i=1}^{S} \frac{H_i^2}{G_i + \lambda} + \gamma^S + d \quad (14)$$

K_{min} is he minimum value of the XGBoost objective function after optimization at a given iteration. It represents the optimized score for the regression trees when both loss and regularization are considered. $\sum_{i=1}^{S}$ is Summation over all leaf nodes in the regression tree. S is the total number of leaf nodes in the current regression tree.H_i is the sum of first-order gradients (errors) of all training samples assigned to the leaf node i. G_i is the sum of second-order gradients (curvatures) of all training samples assigned to leaf node i. λ is a regularization coefficient that controls the magnitude of leaf weights.

Therefore, the XGBoost model combines gradient-based optimization and tree-based ensemble learning to give accurate spectrum detection when combined with SVM.

Support vector machine (SVM)

An XGBoost is combined with an SVM to enhance the evaluation of classification on complex datasets. Although XGBoost is effective in feature selection and the undermining of weak learners, SVM is used to form the decision boundary that will correctly classify the variables based on the constructed model. SVM enhances XGBoost's boosting mechanism and is especially effective at handling smaller training sets. feature redundancy and enhances data representation. SVM architecture shown in Figure 3 (b).

It also exhibits great generalization. Data points of distinct classes are separated by the SVM decision boundary, known as the hyperplane. The margin is the separation between the support vectors and the hyperplane, whereas the support vectors are the data points that are closest to this hyperplane. Maximizing this margin will grant superior classification generalization. The mathematical expression for the hyperplane (c(w)) is the following equation (15).

$$c(w) = xw_j + a \quad (15)$$

Where the input data vector is denoted by w_j. The bias term is defined by a, while x was the weight vector orthogonal to the hyperplane. The separation between classes is ascertained by the margin that is found by the equation (16).

$$\text{margin} = \frac{2}{\|x\|} + D\sum_{j=1}^{m} \varsigma_{j'} \quad (16)$$

Where the weight vector's norm is $\|x\|$. The user-specified penalty parameter that regulates misclassification tolerance is defined in D. When data cannot be perfectly linearly separated, ς_j is utilized as a slack variable. The number of training samples is denoted by m. In reality, maximizing the margin can simply be minimizing $\|x\|$, but this constitutes an optimization query. The Lagrange multiplier, which adds the restrictions to the objective function with multipliers, can be used to solve this optimization. The final SVM decision was expressed as an equation (17).

$$e(w) = \sum_{j=1}^{M} \alpha_j z_j L(w_j, w) + a \quad (17)$$

Where the Lagrange multipliers (weights given to training samples) are represented by α_j. The j^{th} sample's class label was z_j. The entire number of training samples is denoted by M. The kernel function that transfers data into a greater-dimensional space is defined by $L(w_j, w)$. To process the non-linear separation of the information, we use the Radial Basis Function (RBF) kernel, which is defined as the following equation (18).

$$L(w_j, w) = \exp\left(-\frac{\left||x_j - x|\right|^2}{2\gamma^2}\right) \quad (18)$$

Where $\|x_j - x\|$ were two feature vectors, the Euclidean distance between the two feature vectors and γ is the kernel coefficient determining the flexibility of the decision boundary. SVM uses the improved features to create a strong classification boundary after the boosting stage first eliminates.

3.4.2 Adaptive ant colony optimization (AACO)

The individual ants in the classic Ant Colony Optimization (ACO) algorithm are initially placed randomly on a node at the start. The move by ants selecting the next node (spectrum channel or allocation point) is based on a probabilistic decision rule that is applied in the process of building an optimal solution. Figure 3 (c) shows the architecture of AACO. The probability of an ant l migrating to the following node i at time s when it is at a spectrum node j is expressed as follows in equation (19).

$$o_{ji}^{l}(s) = \begin{cases} \frac{S_{ji}^{\alpha}(s)\eta_{ji}^{\beta}(s)}{\sum_{k\in allowed_l} S_{ji}^{\alpha}(s)\eta_{ji}^{\beta}(s)}, & \text{if } i \in \text{allowed}_l \\ 0, & \text{otherwise} \end{cases} \quad (19)$$

$o_{ji}^{l}(s)$ is the transition probability for ant l from node j to node i at time s, $S_{ji}^{\alpha}(s)$ ($\equiv \tau_{ji}(s)$: pheromone intensity on edge (j, i) at time s, $\eta_{ji}^{\beta}(s)$is the heuristic value for moving j → i at time s. α pheromone influence exponent, β is heuristic influence exponent, allowed_l is a set of feasible/unvisited next nodes for ant l, j current node; i candidate next node; k: index over allowed_l, l is ant index, s is time/iteration step

O is the Probability of ant, $\tau_{ji}(s)$ depicts the Pheromone intensity on the spectrum path (j, i) at time s. represents previous allocations that were successful. allowed_l is the set of unvisited spectrum nodes available for ant l. The control parameter that determines the pheromone trail's influence is α. The control parameter that specifies the influence of heuristic information is denoted by β. The modified heuristic factor is as follows in equation (20).

$$\eta_i = \frac{1}{\min[dis(j,i)+dis(i,n)]} \quad (20)$$

η_i is the heuristic factor that guides ant l toward node i. dis(j, i) represents the interference-aware cost between the current allocation (j) and the subsequent allocation (i). Where the distance between i and the final destination allocation m is denoted by dis(i, n). Equation (19) can be substituted into equation (20) to generate equation (21).

$$o_{ji}^{l}(s) = \begin{cases} \frac{[S_{ji}(s)^{\alpha}]\cdot\left[\frac{1}{\min(dis(j,i)+dis(i,n))}\right]^{\beta}}{\sum_i [S_{jl}(s)^{\alpha}]\cdot\left[\frac{1}{\min(dis(j,i)+dis(i,n))}\right]^{\beta}} & \text{if } i \in \\ 0, & \end{cases}$$

allowed_l (21)

The pheromone track on a pathway of the spectrum depletes with time. The updating of the trail intensity after time s is performed as follows equations (22-23).

$$\tau_{ji}(s+t) = \rho\tau_{ji}(s) + \Delta\tau_{ji} \quad (22)$$

$$\Delta\tau_{ji} = \sum_{l=1}^{m} \Delta\tau^{l}{}_{ji} \quad (23)$$

The pheromone deposit by ant l on allocation path (j, i) is represented by $\Delta\tau_{ji}^{l}$, whereas ρ is the pheromone evaporating coefficient (0–1). $\tau_{ji}(s+t)$ is the updated pheromone intensity. For pheromone updates, it employs the ant-cycle system, as defined in equation (24).

$$\Delta S_{ji}^{l} = \begin{cases} \frac{R}{K_l}, & \text{if path } (j,i) \text{ belongs to the best allocation tour} \\ 0, & \text{otherwise} \end{cases} \quad (24)$$

Where K_l is the allocation cost of ant K and R is the total pheromone constant.

AACO is ideal for this domain because its pheromone-driven adaptive search dynamically responds to fluctuating spectrum conditions, balances exploration and exploitation, and handles noisy distributed IoT data. Unlike Bayesian or grid search, AACO avoids local minima and efficiently tunes hyperparameters, giving superior performance within the FedAvg decentralized framework.

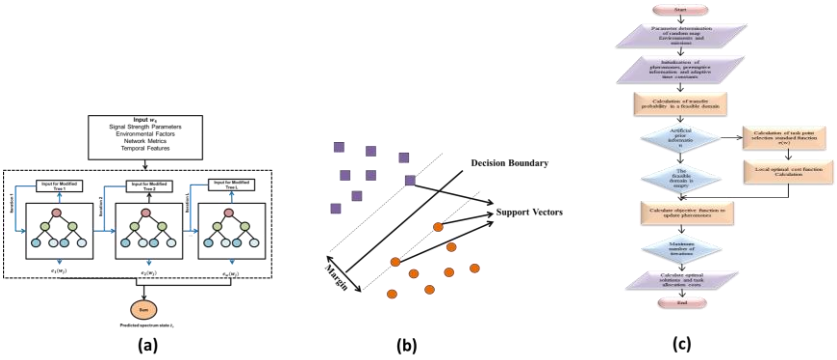

Figure 3: Visualization of (a) XGBoost regression tree model's schematic illustration for spectrum sensing. (b) Support vector machine (SVM) architecture and (c)Flow for Adaptive ACO architecture

The EGSV-AACO combines Extreme Gradient Boosting to refine the features, Support Vector Machine to perform resistant classification, and Adaptive Ant Colony Optimization to optimally tune the hyperparameters. This hybrid scheme expands on accuracy, maximizes the decision boundary, and increases generalization in nonlinear, high-dimensional, and complex datasets. Table 3 demonstrates the Hyperparameters in EGSV-AACO were tuned to optimize spectrum detection accuracy, reliability, and generalization for efficient IoT spectrum sensing.

Table 3: Key hyperparameters of the EGSV-AACO hybrid model

Hyperparameter	Values	Hyperparameter	Values
Learning Rate (α)	0.1	Penalty Parameter (D)	1.0
Number of Trees (L)	100	Pheromone Evaporation (ρ)	0.5
Regularization λ	1.0	Heuristic Influence (β)	2.0
Kernel function	0.001 to 1	Pheromone Influence (α)	1.0

4 Result and discussion

The proposed EGSV-AACO framework for intelligent spectrum sensing and dynamic sharing in IoT networks was implemented on an Intel® Core™ i7-12700K (3.6 GHz) with 32 GB RAM, with GPU support and MATLAB R2022b for simulation and performance evaluation. The findings reveal that it is effective in ensuring effective use of spectrum, speed of access convergence, and secure communication among the IoT devices. The four primary spectrum sensing characteristics are SNR SU1, frequency band, PU presence and PU signal strength. PU appearance is binary (0 or 1) that demonstrates the existence or lack of a primary user. PU presence is binary and with either 0 or 1 that denotes the presence or not of a main user. PU signal strength ranges from around -90 dBm to -40 dBm, indicating clear clustering. The Frequency Band is divided into separate levels around 2000, 3000, 4000, and 5000 MHz. SNR SU1 rises continuously between 5 and 30 decibels, resulting in a dense scatter pattern. Figure 4 illustrates the key spectrum sensing features and their distributions. Figure 4(a) demonstrates substantial clustering and feature separability, enabling the proposed model to achieve accurate spectrum classification. The relation of size of the cluster (3-14) versus the probability of detection (Pd). Pd values are between 0.80 and 0.99, which means that the detection efficiency is always highly effective regardless of the cluster size, as Figure 4 (b) shows. As cluster size grows, Pd values stay tightly distributed between 0.90 and 0.98, indicating high detection reliability. The bulk of points cluster in the top range, implying that larger clusters have a higher detection chance. In general, the results indicate consistent and successful performance in the detection regardless of the size of the cluster, and the lowest Pd is 0.85. The proposed EGSV-AACO model achieves high, consistent detection (Pd 0.85–0.99) across all cluster sizes, ensuring reliable spectrum sensing.

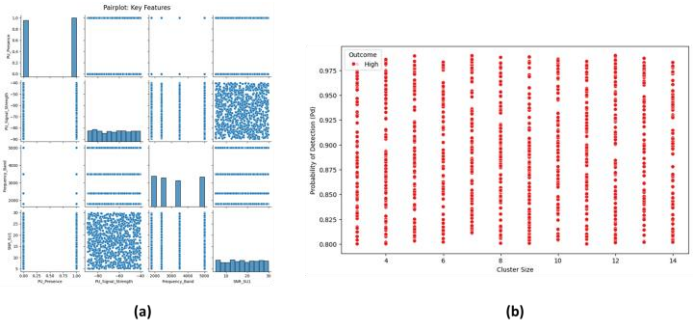

Figure 4: Graphical Representation of (a) Feature Correlation Analysis for Spectrum Sensing Parameters (b) High Detection Performance across Varying Cluster Sizes.

The maximum density lies within the range of Cluster ID that falls within 10-30 and the Frequency Band values that lie within the range of 200-400MHz indicating that the concentration of signals is high within this band. Moderate density also appears around Cluster ID values 35–50 with higher frequency bands (450–600 MHz). The distribution suggests that as Cluster ID increases, signals tend to occupy wider frequency bands, as shown in Figure 5 (a). This supports the purpose of spectrum analysis, highlighting how cluster-based identification can reveal underlying patterns of frequency utilization and potential interference hotspots. The results indicate that the proposed model is successful in identifying, and predicting the presence of spectrum patterns, as well as identifying possible interference.

The relationship between Probability of Detection (Pd) and Probability of False Alarm (Pfa). The scatter distribution shows Pd values ranging from 0.80 to 0.98 and Pfa values from 0.00 to 0.10, as shown in Figure 5 (b). The marginal histograms indicate a high density of Pd values around 0.90–0.95, while Pfa values are concentrated between 0.02–0.06. This shows that the proposed spectrum sensing approach is robust since it has demonstrated good detection performance and low false alarm rates. The mesh-like visualization highlights fluctuations in predicted gaps across varying spectrum bands and signal strengths. Figure 5 (c) illustrates a 3D Wireframe Plot mapping Frequency Band for the proposed model accurately predicts gaps based on spectrum conditions. PU Signal Strength, and Predicted Gap. This high concentration of the wireframe indicates high interdependence with the larger the PU Signal Strength, the larger the gap that is expected to be predicted. In the meantime, the changes in frequencies of moderate frequencies show various results, which means that the system is sensitive to the conditions of channels. That reinforces the importance of spectrum-aware prediction in improving accuracy and reliability in cognitive radio networks systems.

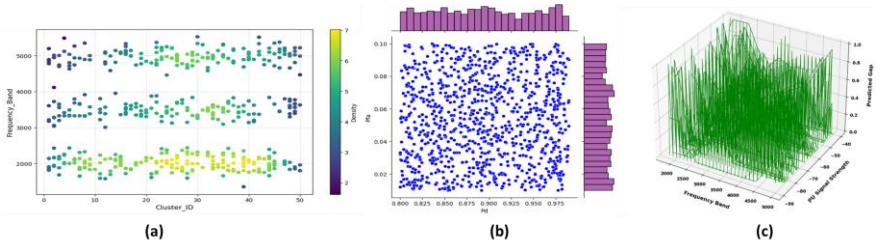

Figure 5: Graphical Representation of the (a) Density Distribution of Cluster ID and Frequency band (b) Joint Distribution Analysis of Pd and Pfa and (c) 3D Wireframe Plot of Frequency Band, PU Signal Strength, and Predicted Gap

The 3D bubble map represents a combination of the analysis of the three SNR features in different cluster sizes and target labels. Maximum clustering is found at SNR_SU1 and SNR_SU2 of between 5 to 15 dB with SNR_SU3 falling within the 0 to 10 dB range meaning that most of the communication states are represented in these ranges. Figure 6 (a) illustrates the relationship between SNR values across secondary users (SU1, SU2, and SU3). Larger bubbles, representing greater Cluster_Size, are concentrated around mid-range SNR values, suggesting that cooperative sensing performs more reliably under moderate channel quality conditions. The color variation (mapped to the Target label) highlights group separations, confirming that performance of the proposed model reliably performs cooperative sensing, with mid-range SNR clusters yielding accurate spectrum detection. Histogram of Probability of Detection (Pd) values of two target classes (0 and 1). The Pd values are between 0.80 and 0.98 with a range of 70 and 115 counts across bins. Class 0 (blue) sustains maximum frequencies that peak at above 100 counts, whereas class 1 (orange) has a range of 17-39 counts, as shown in Figure 6 (b). Both classes possess thicker distributions in the Pd range 0.85-0.90

and 0.95-0.98, The proposed model demonstrates strong target-discriminative detection, maintaining high Pd values (0.80–0.98) across both classes.

The connection between SNR_SU1 (5-30) and SNR_SU2 (5-30). The data points are separated into two groups: blue and red, which represent different target classes. Figure 6 (c) illustrates class is denser in the low to medium SNR_SU1 range (5-15), but the red class dominates at higher SNR_SU1 values (18-30). These two classes are uniformly spread across the SNR_SU2 values with most of them being between 10 25 which suggests a distinct separation along the SNRSU1 axis.

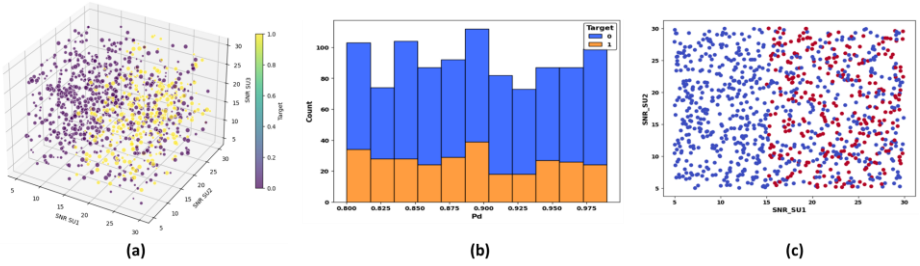

Figure 6: (a) SNR values across secondary users (SU1, SU2, and SU3) and (b) Target-Wise Distribution of Probability of Detection (Pd) and (c) Scatter Distribution of SNR_SU1 and SNR_SU2 across Target Classes

The heatmap shows correlations between spectrum sensing features. PU_Presence is powerfully negatively interrelated with Predicted_Gap (-0.66) and Target (-0.66). SNR_SU1 has a moderate positive association with Predicted_Gap (0.43) and Target (0.43), however, other SNR values (SNR_SU2, SNR_SU3) are barely connected. Figure 7 (a) shows the proposed model relies on key features, with few variables strongly influencing predictions. Most characteristics, including Pd, Pfa, Pmd, Cluster_ID, and Cluster_Size, have correlations between 0.00 and 0.06, showing independence. Strong diagonal values of 1.00 indicate complete self-correlation. This shows that a small number of variables have a large impact on prediction outcomes.

The arrangement of the distribution of the samples in four frequency bands. The band with the largest number is 1800 MHZ with approximately 268 samples, then 5000 MHZ with about 258 samples, as shown in Figure 7(b). The 2400 MHz band includes around 250 samples, whereas the 3500 MHz band has the fewest, with approximately 227 samples. Overall, the dataset is reasonably balanced across frequency bands, with variations of fewer than 40 samples, ensuring a reliable representation for spectrum sensing analysis

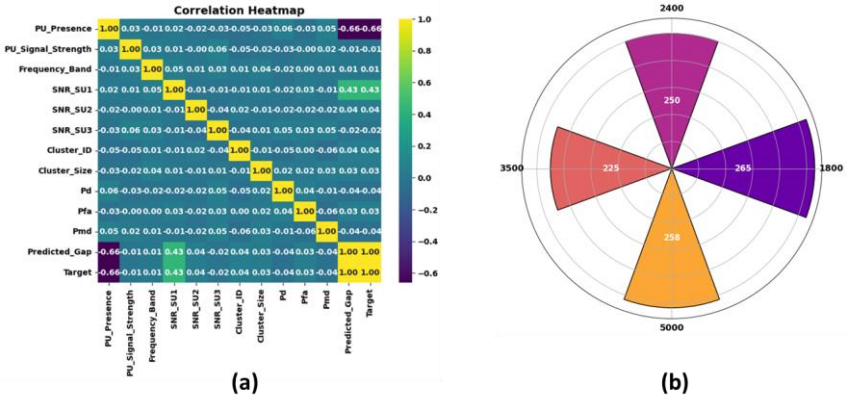

Figure 7: Graphical Representation of (a) Correlation Analysis of Spectrum Sensing Features (b) Sample Distribution Across Frequency Bands

4.1 Comparative analysis result

The proposed model was contrasted with traditional techniques such as DT [26], RF [26], ANN [26], SVM [26], and Seg-CR-VANET [27] in terms of, precision, F1 score, accuracy and recall. The evaluation shows that it performs better than expected in each of these important parameters. Precision shows how consistently the model detects actually idle spectrum without false alarms, and accuracy shows how correctly spectrum sensing judgments are made overall, as shown in Figure 8. F1-score reaches a compromise between precision and recall to provide reliable performance. Recall quantifies the capacity to identify every accessible idle channel, as shown in the intent of attaining dependable, effective, and privacy-preserving spectrum sensing and sharing in IoT networks is validated by these parameters taken together. Table 4 depicts the performance of the different spectrum sensing approaches to IoT communication.

Table 4: Comparative performance metrics of traditional and advanced IoV spectrum methods

Methods	Precision (%)	F1 score (%)	Accuracy (%)	Recall (%)
SVM [26]	94	93	92	92
RF [26]	97	93	92	92
DT [26]	93	91	90	90
ANN [26]	93	91	90	90
Seg-CR-VANET [27]	93.67	93.98	94	94.3
EGSV-AACO [Proposed method]	97.5	96.5	97	96

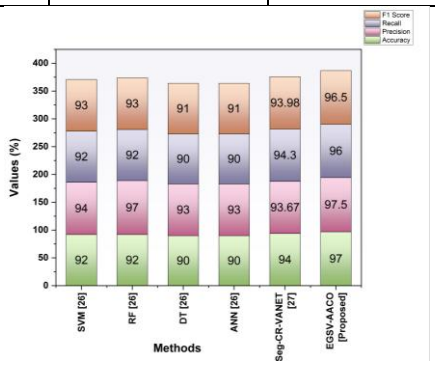

Figure 8: Performance evaluation of spectrum sensing techniques in iot communication precision, accuracy and F1 score, Recall

Traditional models such as SVM [26], RF [26], DT [26], ANN [26], and Seg-CR-VANET [27] achieved accuracy between 90 and 97%, with precision and recall ranging from 90 to 96%. In contrast, the proposed EGSV-AACO technique outperformed all others, achieving 97.5% precision, 96.5% F1-score, 97% accuracy, and 96% recall. In particular, it achieved accuracy improvement over conventional techniques and thus has a high detection reliability and efficiency in dynamic IoT spectrum sensing and sharing.

The EGSV-AACO with FedAvg can effectively address the weakness of the current approaches by incorporating optimal spectrum sensing and cooperation with adaptive optimization and privacy protection. EGSV provides the accuracy of detected idle bands, whereas AACO optimizes hyperparameters in real-time for handling spectrum variability. In contrast to classic centralized approaches, FedAvg eliminates exposure to raw data and offers security and scalability of IoT distributed devices. The hybrid model allows allocating the spectrum swiftly and efficiently, without collisions, and to communicating in a secure fashion, thus making it ideal in highly dynamic IoT ecosystem contexts.

70% training and 30% testing the dataset was spitted. Five-fold cross-validation was applied to ensure robustness, and the table presents standard deviation, 95% confidence intervals, mean, and p-values (Precision: 0.028, Accuracy: 0.032, F1-Score: 0.035, Recall: 0.041,), demonstrating the statistical significance of the EGSV-AACO model's performance. Table 5 shows the **statistical Analysis of EGSV-AACO Model**

Table 5: Statistical Analysis of EGSV-AACO Model with 70:30 Split Cross-Validation

Metric	**Accuracy (%)**	**Precision (%)**	**Recall (%)**	**F1-Score (%)**
Mean	97.0	97.5	96.1	96.8
Std Dev	0.15	0.15	0.15	0.15
95% CI	[96.7–97.3]	[97.2–97.8]	[95.8–96.4]	[96.5–97.1]
p-value	0.032	0.028	0.041	0.035

Ablation study

An ablation study evaluates the impact of each model component by removing or isolating them. Table 6 shows the how EGSV and AACO individually and jointly improve spectrum sensing and sharing.

Table 6: Ablation Study of EGSV-AACO Modules

Model Variant	Accuracy (%)	Precision (%)	Recall (%)	F1-Score (%)
EGSV only	91	92	90	91
AACO only	88	89	87	88
EGSV + AACO	97	97.5	96	96.5

Table 6 demonstrates the EGSV predicts spectrum occupancy accurately, AACO optimizes allocation combined EGSV + AACO achieves best performance (Accuracy: 97%, Precision: 97.5%, Recall: 96%, F1: 96.5%).

4.2 Discussion

Evaluation presents an intelligent, decentralized, and privacy-preserving solution to spectrum sensing and sharing in IoT networks. Each of the existing approaches has certain limitations that make it less effective in dynamic, large-scale, and privacy-sensitive cases of IoT spectrum management scenarios. SVM [26] was incompatible with large volumes of IoT data, expensive to implement as a result of a non-linear kernel, and physically inappropriate in real-time/decentralized environments due to its lack of flexibility in a dynamic spectrum with high probabilities needed to cover temporal change overheads. RF [26] has sufficient accuracy but is very memory-intensive, takes longer to predict with large ensembles, is not flexible to non-stationary spectrum setups, and does not offer natural privacy-preserving measures in large distributed IoT-based networks. DT [26] was straightforward but can easily overfit, has low accuracy towards high-dimensional dynamic spectrum tasks, small generalization strength, and was also weak in a noisy environment due to IoT signals. ANNs [26] are data-hungry, computationally costly, prone to overfitting, not so interpretable, and cannot be readily integrated with privacy-preserving systems in decentralized schemes of IoT spectrum management. Seg-CR-VANET [27] enhanced spectrum assignment in vehicular networks, yet the overhead is high, adaptability to heterogeneous IoT devices or is lacking, and privacy protection is poor due to the federated and data-intensive architecture. The proposed EGSV-AACO framework addresses the limitations of existing methods by combining enhanced global, spatial, -related features with an adaptive ant colony optimization strategy. This integration allows dynamic tuning of parameters, faster and more reliable convergence, improved spectrum detection accuracy, and stronger resilience in complex VANET and IoT scenarios, ensuring efficient, decentralized, and privacy-preserving spectrum allocation

5 Conclusion

Research was developing a decentralized, intelligent, and privacy-preserving framework for spectrum sensing and dynamic sharing in IoT networks. The methodology combined EGSV-AACO for local spectrum detection and FedAvg for secure global aggregation. The research employed a Cognitive Radio Network (CRN) spectrum sensing dataset, incorporating features such as RSSI, SNR, PSD, interference levels, and temporal usage. Data preprocessing was carried out using Min-Max normalization to standardize features. FedAvg enabled collaborative optimization without exposing raw data, ensuring privacy preservation across IoT devices. Experimental results demonstrated that the proposed model achieved 97% accuracy, 97.5% precision, 96% recall, and a 96.5% F1-score, outperforming conventional approaches. The scientific contribution of this reserach lies in the development of a hybrid decentralized learning model that enhances detection reliability and spectrum allocation efficiency. The practical contribution includes enabling secure, scalable, and efficient spectrum sharing in dynamic IoT environments, supporting real-time communication without compromising privacy.

5.1 Limitations and future direction

The weakness of this approach is that it might have scaling problems in highly dense IoT networks, higher computational cost during real-time adaptation, and dependence on stable communication links. Future work will focus on integrating lightweight optimization methods, edge-assisted coordination, and adaptive model compression to reduce computation, improve scalability, and enhance communication resilience for large-scale IoT deployments. Real IoT devices were not emulated, in future work may include real-time testing with defined cluster sizes. Potential future applications include low-latency IoT-enabled patient monitoring in healthcare and collision-free communication in smart transportation systems, where secure and efficient spectrum sharing can enhance reliability and safety.

Author contributions

Jing Ling writing original draft preparation & methodology, Jing Ling investigation & writing review and editing.

References

[1] Lopez, C. A., Castillo, L. F., & Corchado, J. M. (2021). Discovering the value creation system in IoT ecosystems. *Sensors, 21*(2), 328. doi: https://doi.org/10.3390/s21020328

[2] Huo, X., & Wang, X. (2025). A deep learning-driven bidirectional power dispatch optimization framework for smart grids using IoT sensing data. *Informatica, 49*(26). doi: https://doi.org/10.31449/inf.v49i26.8524

[3] Alam, T. (2023). A reliable communication framework and its use in the Internet of Things (IoT). *Authorea Preprints.* doi: https://doi.org/10.36227/techrxiv.12657158.v1

[4] Li, Y. (2024). Construction and monitoring of a quantitative inversion model for conductivity using unmanned aerial vehicle remote sensing based on ELM algorithm. *Informatica, 48*(16). doi: https://doi.org/10.31449/inf.v48i16.6389

[5] Jaramillo-Ramirez, D., & Perez, M. (2021). Spectrum demand forecasting for IoT services. *Future Internet , 13*(9), 232. doi: https://doi.org/10.3390/fi13090232

[6] Chao, J., & Jiao, M. (2025). Network spectrum resource allocation and optimization based on deep learning and TRDM. *Informatica, 49*(13). doi: https://doi.org/10.31449/inf.v49i13.7374

[7] Nasser, A., Al Haj Hassan, H., Abou Chaaya, J., Mansour, A., & Yao, K. C. (2021). Spectrum sensing for cognitive radio: Recent advances and future challeng

es. *Sensors, 21*(7), 2408. doi: https://doi.org/10.3390/s21072408

[8] Fernando, X., & Lăzăroiu, G. (2023). Spectrum sensing, clustering algorithms, and energy-harvesting technology for cognitive-radio-based Internet-of-Things networks. *Sensors, 23*(18), 7792. doi: https://doi.org/10.3390/s23187792

[9] Ali, M., Yasir, M. N., Bhatti, D. M. S., & Nam, H. (2022). Optimization of spectrum utilization efficiency in cognitive radio networks. *IEEE Wireless Communications Letters, 12*(3), 426–430. doi: https://doi.org/10.1109/LWC.2022.3229110

[10] Liu, S., Pan, C., Zhang, C., Yang, F., & Song, J. (2023). Dynamic spectrum sharing based on deep reinforcement learning in mobile communication systems. *Sensors, 23*(5), 2622. doi: https://doi.org/10.3390/s23052622

[11] Biswas, D., Neuwirth, S., Paul, A. K., & Butt, A. R. (2021). Bridging network and parallel I/O research for improving data-intensive distributed applications. *2021 IEEE Workshop on Innovating the Network for Data-Intensive Science (INDIS)* (pp. 50–56). IEEE. doi: https://doi.org/10.1109/INDIS54524.2021.00011

[12] Wang, Y., Li, X., Wan, P., & Shao, R. (2021). Intelligent dynamic spectrum access using deep reinforcement learning for VANETs. *IEEE Sensors Journal, 21*(14), 15554–15563. doi: https://doi.org/10.1109/JSEN.2021.3056463

[13] Grissa, M., Yavuz, A. A., Hamdaoui, B., & Tirupathi, C. (2021). Anonymous dynamic spectrum access and sharing mechanisms for the CBRS band. *IEEE Access, 9*, 33860–33879. doi: https://doi.org/10.1109/ACCESS.2021.3061706

[14] Chang, H. H., Song, Y., Doan, T. T., & Liu, L. (2023). Federated multi-agent deep reinforcement learning (Fed-MADRL) for dynamic spectrum access. *IEEE Transactions on Wireless Communications, 22*(8), 5337–5348. doi: https://doi.org/10.1109/TWC.2022.3233436

[15] Kaur, A., Thakur, J., Thakur, M., Kumar, K., Prakash, A., & Tripathi, R. (2023). Deep recurrent reinforcement learning-based distributed dynamic spectrum access in multichannel wireless networks with imperfect feedback. *IEEE Transactions on Cognitive Communications and Networking, 9*(2), 281–292. doi: https://doi.org/10.1109/TCCN.2023.3234276

[16] Zhang, S., Ni, Z., Kuang, L., Jiang, C., & Zhao, X. (2023). Traffic priority-aware multi-user distributed dynamic spectrum access: A multi-agent deep RL approach. *IEEE Transactions on Cognitive Communications and Networking, 9*(6), 1454–1471. doi: https://doi.org/10.1109/TCCN.2023.3307944

[17] Amrallah, A., Mohamed, E. M., Tran, G. K., & Sakaguchi, K. (2021). Enhanced dynamic spectrum access in UAV wireless networks for post-disaster area surveillance: A multi-player multi-armed bandit approach. *Sensors, 21*(23), 7855. doi: https://doi.org/10.3390/s21237855

[18] Makhdomi, A. A., & Begh, G. R. (2022). Blockchain-based scalable model for secure dynamic spectrum access. *Physical Communication, 55*, 101874. doi: https://doi.org/10.1016/j.phycom.2022.101874

[19] Chen, Y., Wang, Y., Zhang, J., & Di Renzo, M. (2021). QoS-driven spectrum sharing for reconfigurable intelligent surfaces (RISs)-aided vehicular networks. *IEEE Transactions on Wireless Communications, 20*(9), 5969–5985. doi: https://doi.org/10.1109/TWC.2021.3071332

[20] Gu, P., Li, R., Hua, C., & Tafazolli, R. (2021). Dynamic cooperative spectrum sharing in a multi-beam LEO–GEO co-existing satellite system. *IEEE Transactions on Wireless Communications, 21*(2), 1170–1182. doi: https://doi.org/10.1109/TWC.2021.3102704

[21] Kazemi, N., & Azghani, M. (2024). Secure spectrum sharing and power allocation by multi-agent reinforcement learning. *Digital Signal Processing, 146*, 104369. doi: https://doi.org/10.1016/j.dsp.2023.104369

[22] Alipour-Fanid, A., Dabaghchian, M., Jiao, L., & Zeng, K. (2024). Learning-based secure spectrum sharing for intelligent IoT networks. *2024 25th International Symposium on Quality Electronic Design (ISQED)* (pp. 1–8). IEEE. doi: https://doi.org/10.1109/ISQED60706.2024.10528684

[23] Raja, K., Kottursamy, K., Ravichandran, V., Balaganesh, S., Dev, K., Nkenyereye, L., & Raja, G. 2024. An efficient 6G federated learning-enabled energy-efficient scheme for UAV deployment. *IEEE Transactions on Vehicular Technology*, 74(2), 2057-2066. 10.1109/TVT.2024.3390226

[24] Li, L., Xie, W., & Zhou, X. 2023. Cooperative spectrum sensing based on LSTM-CNN combination network in cognitive radio system. *IEEE Access, 11*, 87615-87625. 10.1109/ACCESS.2023.3305483

[25] Okegbile, S. D., & Maharaj, B. T. (2021). Age of information and success probability analysis in hybrid spectrum access-based massive cognitive radio networks. *Applied Sciences, 11*(4), 1940. doi: https://doi.org/10.3390/app11041940

[26] Baiyekusi, O., Mahmoud, H., Mi, D., Arshad, J., Adeyemi-Ejeye, F., & Lee, H. (2024). An ML-based spectrum sharing technique for time-sensitive applications in industrial scenarios. *2024 International Wireless Communications and Mobile Computing (IWCMC)* (pp. 1607–1612). IEEE. doi: https://doi.org/10.1109/IWCMC61514.2024.10592619

[27] Hossain, M. A., Md Noor, R., Yau, K. L. A., Azzuhri, S. R., Z'aba, M. R., Ahmedy, I., & Jabbarpour, M. R. (2021). Machine learning-based cooperative spectrum sensing in dynamic segmentation enabled cognitive radio vehicular network. *Energies, 14*(4), 1169. doi: https://doi.org/10.3390/en14041169